Nigerian Research Journal of Engineering and Environmental Sciences 5(1) 2020 pp. 520-534

Nigerian Research Journal of Engineering and Environmental Sciences
Journal homepage: www.rjees.com

Original Research Article

Preparation, Characterization and Application of Activated Carbon Produced from Rice Husk and Maize Cob for the Adsorption of Disperse Azo Dye in a Fixed Bed

[1]Abdulkareem, K., [2]Iyun, O.R.A. and *[1]Aderemi, B.O.

[1]Department of Chemical Engineering, Ahmadu Bello University, Zaria, Nigeria.
[2]Department of Chemistry, Ahmadu Bello University, Zaria, Nigeria.
*benjaminaderemi@gmail.com

ARTICLE INFORMATION

Article history:
Received 23 Apr, 2020
Revised 01 Jun, 2020
Accepted 02 Jun, 2020
Available online 30 June, 2020

Keywords:
Activated carbon
Disperse azo dye
Dynamic models
Breakthrough curve
Agrowastes

ABSTRACT

In this work, low cost granular activated carbon was produced from maize cob (MC) and rice husk (RH). Calcination of the agrowastes at 500 °C was followed by phosphoric acid (H_3PO_4) treatment. The produced activated carbons (AC) were characterized for surface area and pore size using Brunauer - Emmett-Teller (BET) in a micromeritics ASAP 2020 V_3.04H. The adsorption potential of the granular composite activated carbon (GCAC) for pyridone (a disperse azo dye – $C_{21}H_{14}ClN_5O_5S$) removal from aqueous solution was investigated using a fixed-bed adsorption column. The effects of the inlet dye concentration (50–200 mg/L), feed flow rate (85-115.6 mL/min), activated carbon granular mass (15 - 60 g) and particle size (1.0 – 6.0 mm) on the breakthrough characteristics of the adsorption system were determined. Brunauer -Emmett-Teller (BET) method gave surface area of 796.8 m^2 /g, and average pore size of 32.67 Å for AC produced from 70% maize cob and 30% rice husk. The maximum adsorption capacity of 84.11 mg/g was obtained in the bed using 50 mg/L inlet dye concentration, 20 g adsorbent mass, 85.0 mL/min adsorbate flow rate and 1.0 mm adsorbent particle size for the MC: RH (70:30) combinations. The dynamic adsorption behaviour of the bed was tested using Adams–Bohart, Thomas, and Yoon–Nelson models. Thomas and Yoon-Nelson models displayed R^2 values greater than 96% for most of the points investigated and hence, are preferred in this study. The GCAC was shown to be a suitable adsorbent for adsorption of disperse azo dye in a fixed-bed column system.

1. INTRODUCTION

Increase in human population, industrial and agricultural activities have consequential effect on generation of water pollutants, making wastewater treatment an active research focus worldwide. Water pollution results

from direct or indirect industrial effluents discharge into water bodies without adequate treatment to remove harmful compounds and dyes happened to be one of the major culprits in this regard (Rouf and Nagapadma, 2015).

Dyes are indispensable ingredients of textile and leather industries. They are intensively coloured materials, and therefore cause obnoxious problems in effluent discharge. They are aesthetically displeasing and hazardous to life. In addition, their presence, even in small quantity prevent sunlight penetration, decreasing photosynthetic activity in aquatic environments (Ahmad and Hameed, 2010). There are different types of dyes, and these include, acid, reactive, disperse, vat, metal complex, mordant, direct, basic and azo dyes. Azo dyes are synthetic colors, which contain azo group, -N=N- in their structure. The aromatic side groups around the azo bond help to stabilize the azo group and to produce strong colors. Azo dyes are among the largest group of synthetic dyes commercially produced annually (Ahmad and Hameed, 2010). Disperse azo dyes are free from ionizing group, sparingly soluble in water and are suitable for dyeing hydrophobic textile materials.

Well-known methods for dye removal can be broadly divided into physical, chemical and biological methods. Biological processes using fungi and bacteria are cost effective but the long growth cycle is a disadvantage (Tan *et al*., 2013; Katheresan *et al*., 2018). Physico-chemical methods like coagulation, flocculation, and oxidation are rapid and highly efficient on large scale but with clean separation challenges as its drawback (Merzouk et al., 2011; Katheresan *et al*., 2018). However, it has been reported that adsorption is the best method for removal of azo dye contaminant from wastewater (Yagub *et al.*, 2012; Yagub *et al.*, 2014).

The choice of adsorbent is the most important factor in adsorption (Ranga and Sanghvi, 2015). Available commercial activated carbons (AC) are usually produced from coal and petroleum pitch. Even though these commercially available AC grades have been proven to be effective and versatile as adsorbents due to their high extended surface area, pores structure, high adsorption capacity and high degree of surface reactivity, the high cost associated has always been argued to be a serious drawback (Rahman *et al.,* 2005). In addition, the current strict environmental regulations on net carbon emission and non-renewability of coal and petroleum stock support the intensity shown towards production of AC from agricultural residue currently ongoing in many laboratories worldwide (Vadivelan and Kumar, 2005; Hadi *et al*., 2011).

Biomass waste offers cost effective and renewable source for the production of AC. There are reported works on chemical activation of biomass to improve its pore structure distribution, and consequently enhancing its adsorption characteristics such as the adsorptive capacity and bulk density of the activated carbons produced from lignocellulosic materials (Williams and Reed, 2006; Tay *et al*., 2009; Rouf and Nagapadma, 2015; Shamsuddin et al., 2015; Maneerung *et al*., 2016). Nonetheless, phosphoric acid is the preferred chemical for activation in the current work because of the merit of its efficient recovery and environmental friendliness (Rahman *et al*., 2015; Chen *et al*., 2017). Phosphoric acid activation has been applied to coals and hardwoods (Zhou et al., 2001; Rouf and Nagapadma, 2015), and shells of nuts like almond and pecan (Hadi *et al*., 2011).

Furthermore, most of the studies on adsorption using activated carbon (AC) were conducted in batch operational mode, probably due to the simplicity of the setup and easy of analysis of the isotherm data, including fixing of the adsorption kinetics (Goel *et al*., 2005; Mahmood *et al*., 2011; Nsami and Mbadcam, 2013). However, the bulky nature of the industrial effluents demands investigating into continuous mode adsorption. Hence, studies involving the use of a fixed bed column to predict column breakthrough profile for a novel adsorbent and to determine its operational life span in the bed and regeneration time, and to obtain basic engineering data is indispensable.

In this study therefore, important design parameters such as inlet concentration of dye solution, flow rate, adsorbent weight in the bed and adsorbent particle size were investigated in a laboratory size fixed-bed

column. The breakthrough curves for the adsorption of a disperse azo dye were analyzed using Adam's–Bohart, Thomas and Yoon–Nelson dynamic models.

2. MATERIALS AND METHODS

2.1. Adsorbate

Pyridone ($C_{21}H_{16}ClN_5O_5$, Mw, 485.90 g/mol, Yield, 82%, Mp, 295 °C, R_F 0.89 and molecular wave length (λ_{max}) of 482.97 – a disperse azo dye) used in this study was obtained from Chemistry Department Ahmadu Bello University, Zaria, Nigeria. The dye stock solution was prepared by dissolving accurately weighed dye in distilled water to the concentration of 1 g/L (Ahmad and Hameed 2010). Solutions used for the experiment were obtained by dilution method to produce varying inlet concentrations. The chemical structure of the pyridone dye is shown in Figure 1.

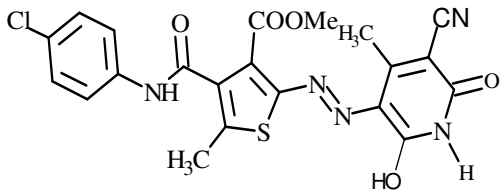

Figure 1: Chemical structure of pyridone

2.2. Preparation of Activated Carbon

Rice husk and maize cob used for the preparation of the granular activated carbon was obtained from a farm near Basawa, Zaria, Kaduna State, Nigeria. They were washed with distilled water to remove dust like impurities, then dried under the sun to constant weight (5 days) and subsequently crushed with pestle and mortar and sieved to the desired particle sizes (1–2 mm).

The thermo-chemical activation method employed involved carbonization of the raw mixture of rice husk and maize cob, and subsequent activation using phosphoric acid (purity 85% Merck, Germany). Four different samples, composed of combined MC and RH in the ratios of 70:30, 30:70; 100:0; and 0:100 respectively, were prepared. In a typical AC sample preparation, 40 g of the precursor was first carbonized at 500 °C for 2 h under nitrogen flow (150 cm^3 /min.) at a heating rate of 10 °C/min. after which the carbonized material was then impregnated with 40 wt. % solution of phosphoric acid (4.5 parts of H_3PO_4 to 1 part of the precursor) with occasional stirring (Dusta *et al*., 2012). The thus activated samples were cooled to room temperature and then washed several times with distilled water until the pH of the washing solution reached 7. Finally, the samples were dried in an oven at 110 °C for 24 h and then stored in plastic containers.

2.3. Preparation of the Granulated Composite Adsorbent

The activated carbon prepared from the mixture of maize cob and rice husk (70:30) was mixed thoroughly with starch in the ratio of 2:1 based on the work of Dusta *et al*. (2012) to give it mechanical strength and to serve as a binder to the powdered activated carbon produced. The resulting granular composite activated carbon pellets (GCACP) were then cooled to room temperature and stored in a desiccator for characterization and application in dye removal.

2.4. Physical and Chemical Characterization

Proximate analysis was employed in determining the moisture content, volatile matters, fixed carbon, and ash residues of the precursor (mixture of rice husk and maize cob) and the composite activated carbon. Ultimate analysis was done using the Elemental Analyzer to evaluate the percentage of carbon, hydrogen, and oxygen present in the samples. The surface chemistry of the samples was analysed by identifying the surface functional groups using Fourier transform infrared spectroscope (FTIR- 2000, Perkin Elmer). The spectral were recorded from 4000 to 500 cm^{-1} resolution in the mid- infrared region. Nitrogen adsorption at 77 K (liquid nitrogen) was conducted using a micromeritics ASAP 2020 V_3.04H (micromeritics®), to obtain the adsorption isotherm of the samples. The Brunauer- Emmett-Teller (BET) method was used to calculate the specific surface area of the prepared activated carbon powder from the isotherms. All samples were degassed at 350 °C for 6 hours prior to analysis.

2.5. Adsorption Experiments

The fixed-bed column was made of Pyrex glass tube of 2.0 cm inner diameter and 17 cm height schematically shown as Figure 2. The column was packed with the GCACP connected to an adjustable pump for uniform flow of solution. To avoid entrapping of air bubbles inside the GCAC pellets, the particles were soaked in appropriate amount of water and agitated until no air bubbles were detected in the solution. GCACP particle size of 1.0 mm – 6.0 mm; mass of 15 – 60 g was packed in the column as fixed beds with the support of glass wool at the bottom of the column. Dye solution of known concentrations 50 – 200 mg/L was allowed to flow through the column at flow rates of 85.0, 110.55, and 115.6 mL/min. The aliquot of the disperse azo dye solution was collected at the outlet of the column at regular time intervals and its residual absorbance was measured using a double beam UV–visible spectrophotometer (Spectra scan UV 2600) at 482.97 nm and the residual dye concentration was determined from a pre-calibrated absorbance - concentration graph. All experiments were carried out at temperature of 25±3 °C.

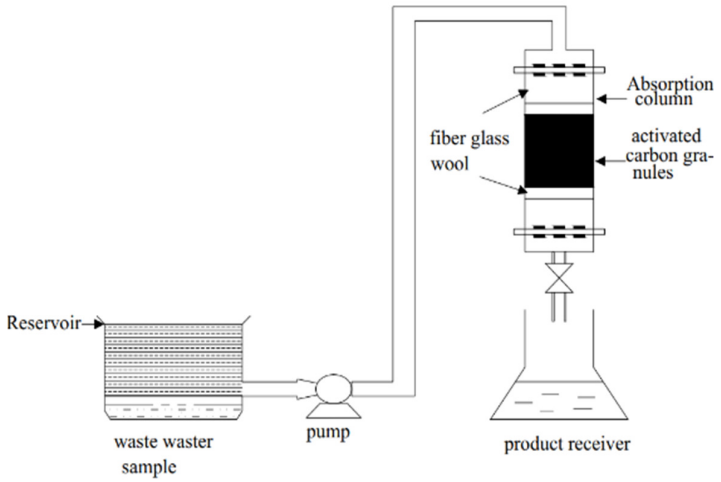

Figure 2: Schematic diagram of the dye adsorption experimental set up

2.6. Analysis of Fixed Bed Column Data

Equations 1-5 were used to determine the efficiency of the fixed bed.

$$V_{eff} = Qt_{total} \tag{1}$$

V_{eff} is the effluent volume, t_{total} and Q are the total time of flow (min) and volumetric flow rate (mL/min) respectively.

The area under the breakthrough curve (A) obtained by integrating the adsorbed concentration (C_{ad}, mg/L) versus time t(min) (presented as Equation (2)) was used to find the total adsorbed dye quantity (m_{total}).

$$m_{total} = \frac{Q}{1000}\int_{t=0}^{t=t_{total}} C_{ad}\,dt \tag{2}$$

where C_{ad} is the adsorbed dye concentration (Ahmad and Hameed, 2010).

Maximum capacity (q_{max}) of the column was defined by Equation (3) as the total amount of adsorbed (qt_{total}) per gram of adsorbent (W) at the end of total flow time.

$$q_{\max} = \frac{m_{total}}{W} \tag{3}$$

Where, q_{max} is the maximum dye uptake (mg/g), and W is adsorbent bed weight in the column, (g)

The total amount of dye sent to the column is given by Equation (4).

$$M_{total} = \frac{C_o Q t_{total}}{1000} \tag{4}$$

Where, M_{total} is total amount of dye sent to the column (g), C_o is the initial dye concentration (mg/L), Q is the volumetric flow rate (mL/min), t_{total} is total flow time (min).

Total percentage of dye removal is given by Equation (5).

$$\%removal = \frac{m_{total}}{M_{total}} \times 100 \tag{5}$$

3. RESULTS AND DISCUSSION

3.1. Proximate and Ultimate Analysis

The carbonization process at 500 ^oC reduced the moisture content and volatilities of the raw RH and MC, while the fixed carbon and ash content of the samples increased with phosphoric acid treatment after carbonization as shown in Table 1. Activated carbon is generally priced on a moisture free basis and hence the moisture content must be as low as possible (Zhou *et al.*, 2001; Bernal *et al*, 2018).

The high carbon content of AC produced from mixture of RH and MC is an indication of its suitability for the adsorption purposes. The carbon content of the raw MC + RH (24.35%) increased to 75.10%, while other elements like hydrogen, sulphur and (N+O) reduced due to removal of the light components in the sample during carbonization.

Table 1: Proximate and ultimate analysis of raw mixture of rice husk (RH) and maize cob (MC) and AC produced from mixture of maize cob and rice husk

Samples (%)	Proximate analysis					Ultimate analysis			
	Moisture content	Volatiles	Fixed carbon	Ash	Bulk density (g/mL)	C	H	S	(N+O)+
Raw RH+MC	6.60	58.15	24.35	10.90	1.76	47.42	7.82	0.46	44.40
AC from RH	2.50	0.07	74.81	22.62	3.69	76.98	3.86	0.36	18.98
AC from MC	3.90	0.07	74.69	21.34	2.92	75.86	2.59	0.08	21.47
AC from RH+MC	3.40	0.14	75.10	22.74	6.61	78.58	1.48	0.05	20.89

+ other elements

3.2. Surface Area and Porosity

Surface area analysis presented in Table 2 showed that carbon synthesized during the carbonization and activation with H_3P0_4 from 70% maize cob and 30% rice husk had better surface properties in term of surface area (796.8 m^2/g), pore size (32.69Å), and pore volume of (0.2809 cm^3/g) than that produced from 30% maize cob and 70% rice husk with surface area (753.5 m^2/g), pore size (30.4 Å), and pore volume of (0.2947 cm^3/g). AC produced from maize cob alone had surface area of 365.2 m^2/g, pore size 32.96 Å, and pore volume of 0.2394 cm^3/g and AC produced from rice husk gave surface area (324.5 m^2/g), pore size (30.98 Å), and pore volume of (0.2001 cm^3/g). It is clearly shown that the dehydration process by calcination and chemical activation led to increase in the surface area and porosity, possibly by dissolving salts that may have limited access to the internal network of the AC (Guo and Lua, 2003; Rahman *et al*., 2015; Chen *et al*., 2017).

Table 2: Surface properties of various activated carbon produced from maize cob and rice husk using T-method of external surface area analysis

Adsorbent	Physical properties		
	Specific surface area m^2/g	Pore size (Å)	Pore volume cm^3/g
AC produced from 70% rice husk and 30% maize cob	753.5	30.4	0.2947
AC produced from 70% maize cob and 30 % rice husk	796.8	32.69	0.2809
AC produced from maize cob	365.2	32.96	0.2394
AC produced from rice husk	324.5	30.98	0.2001

3.3. Fourier Transform Infrared (FT-IR) Analysis

The FTIR spectrum obtained for the prepared activated carbon is presented in Figure 3 in comparison to the spectrum obtained for the raw mixture of maize cob and rice husk (Figure 4). The spectrum of the activated carbon (Figure 3) is similar to those shown in the literature for lignocellulosic materials activated by H_3PO_4 (Cibele *et al*., 2013). The bands seen in the region between 1755 and 1650 $cm^{-1,}$ are attributed to C=O stretching vibrations in esters, and bands seen in the region between 1300 and 1000 $cm^{-1}$are attributed to C-O stretching vibrations associated with ethers in the activated carbon (Figure 3) (Chen *et al*., 2017).

Similarly, the band seen in the region between 1300 and 1000 cm^{-1}, with maxima at 1263 cm^{-1} are attributed to C-O stretching vibrations in acids, alcohols, phenols, ethers, and esters in mixture of maize cob and rice husk (Figure 4) (Chen *et al*., 2017).

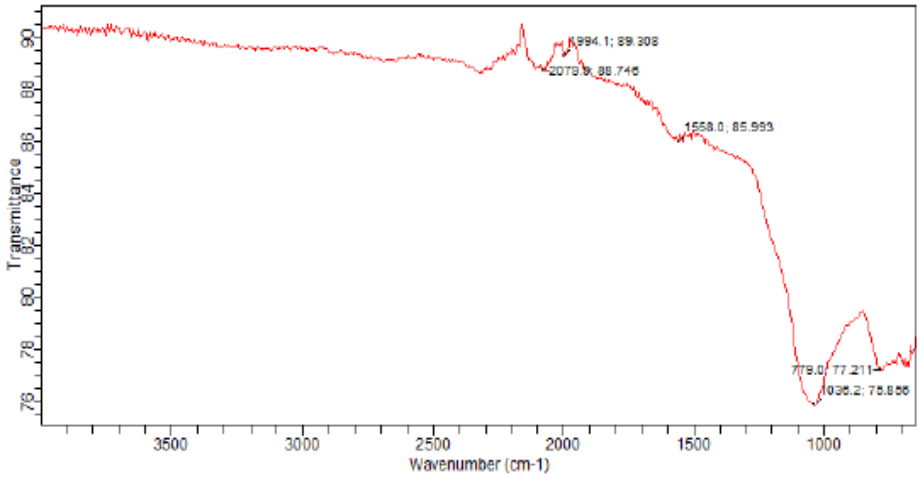

Figure 3: FTIR spectral of activated carbon produced from mixture of rice husk and maize cob

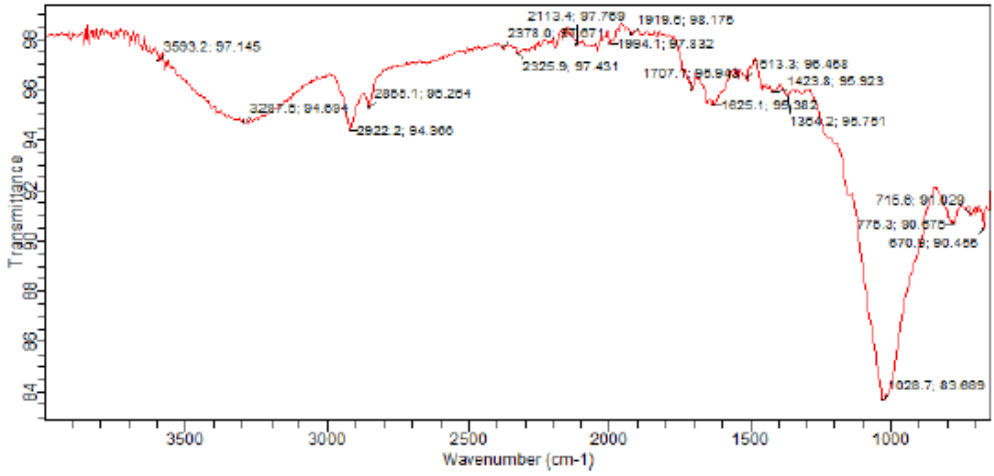

Figure 4: FTIR spectral raw mixture of rice husk and maize cob

The significant difference between these bands confirms the effect of the activation procedure. Bands at 1121 cm^{-1} ($–OCH_3$) and near 1724 cm^{-1} (C=O stretching band) have been reported in association with the presence of lignin and hemicelluloses esters (Cibele *et al*., 2013). It was observed that these bands are less evident in the activated carbon (Figure 3) in comparison to the raw mixture of maize cub and rice husk (Fig 4). This is probably associated with hydrolysis of lignin and hemicellulose constituent esters by the activating agent. The broad bands at 3200–2700 and 3800–3400 cm^{-1} are attributed to hydrogen bonds in carboxylic acid and phenolic groups respectively. Reduction in intensity of such bands after activation could be attributed to interaction between the O–H group and the activating agent (Chen *et al.*, 2017).

3.4. SEM Analysis

The textural structure of the activated carbon obtained from SEM at a magnification of 1500 is shown in Figure 5. It was characterized by irregular and porous surface morphology. The pores were prominent on the activated carbon surface. The pores observed have been attributed to the loss of volatile matter and the effect of activating agent on raw mixture of rice husk and maize cob.

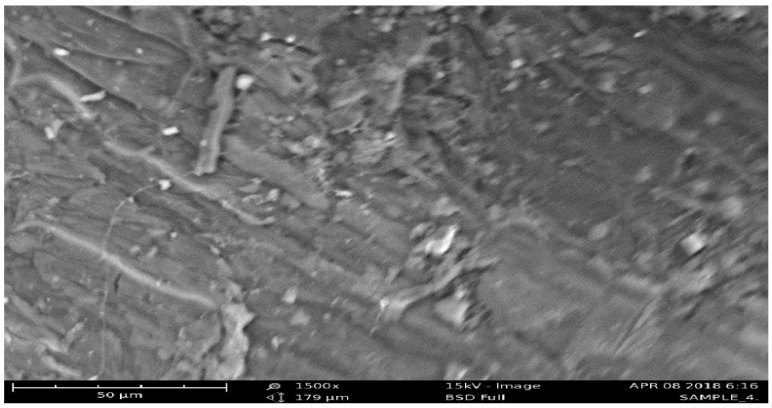

Figure 5: SEM of activated carbon produced from mixture of rice husk and maize cob

3.5. Adsorption Column Studies

Due to limitations inherent in the peristatic pump used, only three flow rates (85.0, 110.5 and 115.6 ml/min) could be investigated in this study. Nonetheless the adsorbate flow rate showed significant effect on the disperse azo dye adsorption in the fixed bed column. The effect of flow rate on breakthrough curve as a function of time is shown in Figure 6.

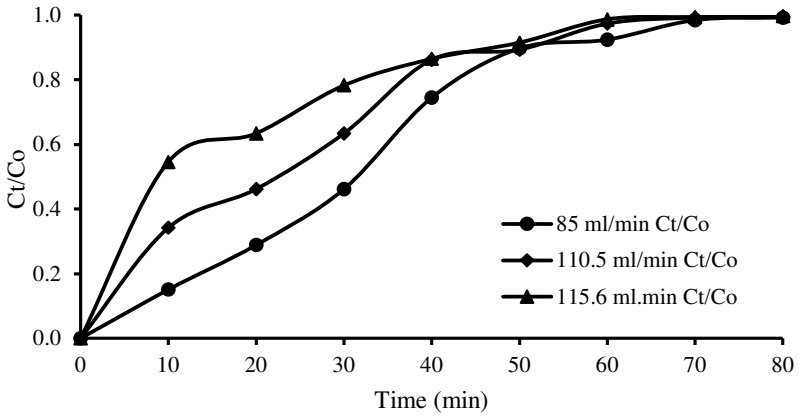

Figure 6: Breakthrough curves for the dispersed azo dye adsorption on prepared GCAC at different flow rates (dye concentration = 50 mg/l, adsorbent mass = 20 g and adsorbent particle size = 4.0 mm

As shown in Figure 6 the breakthrough occurred relatively faster at higher adsorbate flow rate, taking less time to reach saturation breakthrough. This phenomenon can be explained in the understanding that increase in flow rate at constant dye concentration means increase in total dye quantity in a shorter time leading to

quicker bed saturation. Conversely, the adsorption capacity decreased with increase in flow rate due to shorter residence time of the adsorbate molecule in the fixed bed column.

The effect of initial concentration is shown in Figure 7. It was observed that the breakthrough time slightly decreased with increasing inlet concentration. This may be attributed to the fact that at lower inlet concentrations, saturation occurred slowly but with increase in inlet concentration the breakthrough time decreased. This was not unconnected with the fact that the driving force for mass transfer increases with increase in inlet dye concentration which in turn increased the adsorption capacity of the bed due to possibility of multilayer adsorption at high dye concentration (Biswas and Mishra, 2015).

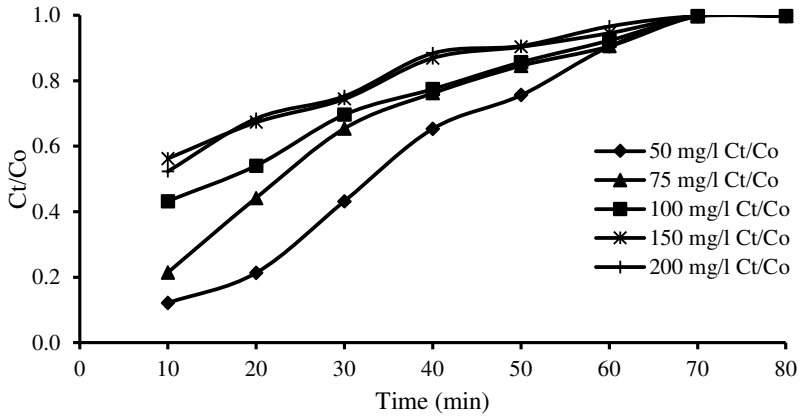

Figure 7: Breakthrough curves for the disperse azo dye adsorption on prepared GCACP at different inlet dye concentrations at inlet flow rate of 85 ml/min and adsorbent mass of 20 g

The effects of increase in adsorbent bed weight and adsorbent particle size with respect to breakthrough of disperse azo dye are shown in Figures 8 and 9. The breakthrough patterns are not too different from the other factors, the 100% breakthroughs occurred at almost same time of 70 mins, for all the conditions studied. The differences in adsorption characteristics are more glaring at the early stages of operation where time, t< 50 mins. Hence, subsequent column analysis was limited to t = 60 mins.

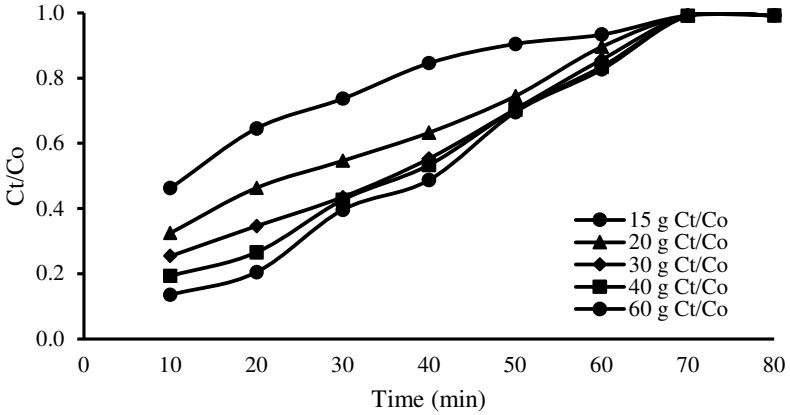

Figure 8: Breakthrough curves for the disperse azo dye adsorption on prepared GCACP at different adsorbent mass, at Co of 50 mg/l, inlet flow rate of 85 ml/min and adsorbent particle size of 4.0 mm

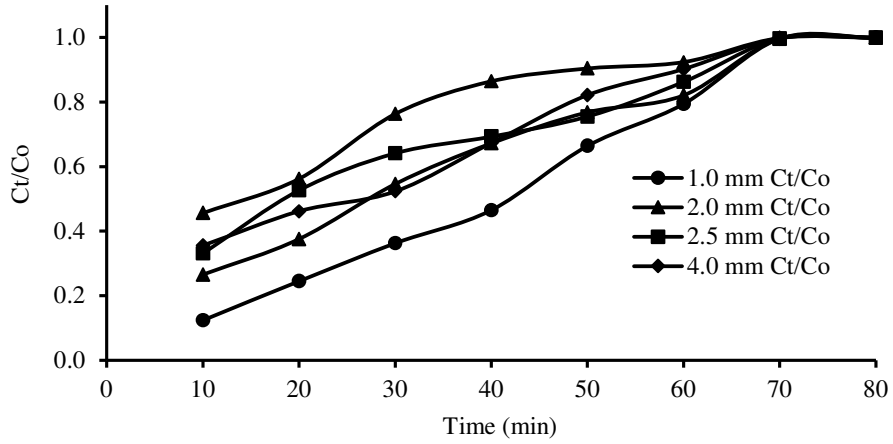

Figure 9: Breakthrough curves for the disperse azo dye adsorption on prepared GCACP at different adsorbent particle sizes at C_o of 50 mg/l, inlet flow rate of 85 ml/min and adsorbent mass of 20 g

Clearly, adsorption of the disperse azo dye studied is more favourable at low flow rate (85 ml/min), high dye concentration (200 mg/l), low particle size (1.0 mm) and high adsorbent mass as evident from Figures 6 to 9 and corroborated by the performance data presented in Table 3.

Table 3: Effect of operation variables on column performance during dye adsorption

Adsorption conditions	q_{max} ($mg_{adsorbate}/g_{adsorbent}$)	Percentage dye removal (%)
Flow rate, 85.0 – 115.5 ml/min	0.1712 – 0. 2017	59.25 – 97.47
Initial dye concentration, 50 – 200 mg/l	0.1918 – 0.2545	29.94 – 90.28
Adsorbent mass, 15 – 60 g	0.2458 – 0.3255	11.57 – 85.32
Adsorbent particle size, 1.0 – 6.0 mm	0.1106 – 0. 1737	52.05 – 81.75

It may be because with the increase in adsorbent bed mass, the adsorbate had more time to interact with the surface of the activated carbon, which in turn resulted in higher dye removal capacity and lower solute concentration in the effluent (Biswas and Mishra, 2015). Besides, at higher adsorbent bed mass, more effective surface area was provided, which offers more active sites to adsorption and it also broaden the mass transfer zone length. The other possible reason may be that at lower adsorbent particle size (large surface area), disperse azo dye had more time to have a contact with the surface of activated carbon in the bed which resulted to less steep-like breakthrough curve (Ghribi and Chlendi, 2011; Mitra et al., 2018; Patel, 2019).

3.6. Dynamic of Adsorption Models

Bohart-Adams, Thomas, and Yoon-Nelson dynamic models are commonly used to describe the performance of adsorption packed columns and to evaluate its specific parameters such as rate constant, adsorption capacities, saturation concentration and time to attain 50% adsorbate breakthrough. The linearized forms of these models are presented as Equations (6-8) (Dusta *et al.*, 2012):

$$\ln\frac{C_t}{C_o} = K_{AB}C_o t - K_{AB}N_o\frac{Z}{F} \quad \text{(Adams - Bohart)} \tag{6}$$

$$\ln\left(\frac{C_o}{C_t}-1\right) = \frac{k_{Th}q_o W}{Q} - k_{Th}C_o t \quad \text{(Thomas Model)} \tag{7}$$

$$\ln\left(\frac{C_t}{C_o - C_t}\right) = k_{YN}t - \tau k_{YN} \qquad \text{(Yoon - Nelson Model)} \tag{8}$$

where C_o and C_t (mg/L) are the inlet and effluent dye concentrations respectively, k_{AB} (L/mg min) is the Adams-Bohart kinetic constant, F (cm/min) is the linear velocity calculated by dividing the flow rate by the column cross sectional area, Z (cm) is the bed depth in the column and N_o (mg/L) is the saturation concentration. *W* is the mass of the adsorbent (g), Q is the volumetric flow rate of adsorbate (mL/min), k_{TH} is the Thomas rate constant, and q_o is the maximum dye adsorption capacity of the adsorbent (mg/g), k_{YN} (min^{-1}) is the rate velocity constant or Yoon–Nelson constant, τ (min) is the time required for 50% adsorbate breakthrough, and *t* is the sampling time.

Column adsorption capacity can easily be evaluated from τ, time for 50% adsorbate breakthrough based on Equation (9).

$$q_{OYN} = \frac{m_{total}}{W} = \frac{C_o Q \tau}{W} \tag{9}$$

Table 4 presents the summary of the column parameters derived from the linear plots of Equations (6 – 8).

From Table 4 (a to c), the Adams-Bohart model displayed R^2 values < 95%, in most of the points investigated, whereas, Thomas and Yoon-Nelson models showed corresponding R^2 values > 96%. The adsorption capacities from the two acceptable models are generally the same for the variables studied. Values of k_{Th} and k_{YN} decreased as the initial disperse azo dye concentration and volumetric flow rate increased. This trend is in agreement with the observation of Yunnen *et al*. (2017) as well as Biswas and Mishra (2015).

However, k_{Th} and k_{YN} values showed initial decrease with increase in adsorbent particle size and adsorbent mass but started rising with increase in the duo variables. The maximum adsorption capacity of the bed, q_{max} (mg/g) decreases with the volumetric flow rate and particle diameter respectively but showed an increasing trend with adsorbent mass, confirming the earlier speculated multilayer adsorption. The increase in adsorption capacity was because the adsorbate has more time to interact with the surface of adsorbent as the adsorbent mass in the bed increased from 15 g to 60 g, which in turn resulted in higher adsorption capacity. Furthermore, as adsorbent bed particle size increased from 1.0 mm to 6.0 mm, adsorption capacity decreases because the available surface area for adsorption decreased.

From Table 4b, as inlet concentration increased from 50 mg/L to 200 mg/L, the value of maximum amount dye uptake per gram of adsorbent (q_0) was sinusoidal but the value of K_{Th} decreased. The reason was that the driving force for adsorption is the concentration differences between the dye on the adsorbent and the dye in the solution. As the flow rate increased from 85.0 mL/min to 115.6 mL/min, the value of q_o decreased but the value of K_{Th}increased,the reason was that the rate of mass transfer get decreased at higher flow rate leading to decrease in amount of dye uptake per gram of the adsorbent. In contrast, as the adsorbent mass increased from 15 g to 60 g, the value of equilibrium amount of dye uptake per gram of adsorbent increased significantly, while the value of K_{Th}decreased, the reason for increased in equilibrium amount of dye uptake per gram was that with increased in adsorbent bed weight the adsorbate has more time to interact with the adsorbent surface, which in turn resulted into higher dye removal.

Table 4a: Summary of column dynamic parameters from Yoon-Nelson model

Dye concentration (mg/l)	Slope	I	R^2	k_{YN} (min^{-1})	ť (min)	q_{max} (mg/g)
50	0.084	2.858	0.993	0.0838	34.1	72.47
75	0.069	1.706	0.975	0.0689	24.76	78.93
100	0.055	0.87	0.995	0.0545	15.96	67.83
150	0.052	0.331	0.989	0.0524	6.323	40.31
200	0.062	0.566	0.976	0.0621	9.11	77.43
Flow rate (ml/min)						
85	0.09	2.662	0.985	0.0901	29.54	62.78
110.5	0.084	1.729	0.97	0.0843	20.51	56.66
115.6	0.077	0.915	0.918	0.0765	11.96	34.55
AC pellet diameter						
1	0.064	2.529	0.993	0.0639	39.58	84.11
2	0.053	1.488	0.989	0.0525	28.35	60.24
2.5	0.046	0.972	0.964	0.0457	21.26	45.17
4	0.056	1.339	0.97	0.0564	23.74	50.46
6	0.057	0.694	0.967	0.0571	12.16	25.83
AC pellet mass (g)						
15	0.056	0.614	0.993	0.0559	10.99	31.13
20	0.053	1.331	0.954	0.0526	25.3	53.76
30	0.055	1.782	0.97	0.0552	32.28	45.73
40	0.061	2.154	0.991	0.061	35.32	37.53
60	0.686	2.617	0.991	0.686	3.815	2.70

Table 4b: Summary of column dynamic parameters from Thomas model

Dye concentration (mg/l)	Slope	Int	R^2	k_{Th} (l/mg.min)	Slope
50	0.084	2.858	0.993	0.00168	72.471
75	0.069	1.706	0.975	0.00092	78.929
100	0.055	0.87	0.995	0.00055	67.828
150	0.052	0.331	0.989	0.00035	40.306
200	0.062	0.566	0.976	0.00031	77.431
Flow rate (ml/min)					
85	0.09	2.662	0.985	0.0018	62.776
110.5	0.084	1.729	0.97	0.00169	56.662
115.6	0.077	0.915	0.918	0.00153	34.552
AC pellet diameter					
1	0.064	2.529	0.993	0.00128	84.112
2	0.053	1.488	0.989	0.00105	60.237
2.5	0.046	0.972	0.964	0.00091	45.174
4	0.056	1.339	0.97	0.00113	50.457
6	0.057	0.694	0.967	0.00114	25.835
AC pellet mass (g)					
15	0.056	0.614	0.993	0.00112	31.126
20	0.053	1.331	0.954	0.00105	53.763
30	0.055	1.782	0.97	0.0011	45.731
40	0.061	2.154	0.991	0.00122	37.525
60	0.686	2.617	0.991	0.01372	2.7026

Table 4c: Summary of column dynamic parameters from Adams-Bohart model

Dye concentration (mg/l)	Slope	Int	R^2	k_{AB} (l/mg.min)	N_o (mg/L)
50	0.041	2.307	0.928	0.00081	563.45
75	0.027	1.484	0.827	0.00035	831.92
100	0.015	0.913	0.944	0.00015	1202.1
150	0.01	0.624	0.942	6.9E-05	1789.9
200	0.012	0.668	0.908	5.8E-05	2289.5
Flow rate (ml/min)					
85	0.037	2.024	0.916	0.00074	543.96
110.5	0.022	1.183	0.924	0.00043	711.75
115.6	0.012	0.675	0.947	0.00024	766.81
AC pellet diameter (mm)					
1	0.036	2.238	0.957	0.00072	621.52
2	0.023	1.429	0.93	0.00046	620.56
2.5	0.017	1.092	0.872	0.00034	638.83
4	0.019	1.189	0.986	0.00038	622.03
6	0.015	0.834	0.877	0.00029	571.59
AC pellet mass (g)					
15	0.013	0.776	0.883	0.00027	579.8
20	0.019	1.225	0.973	0.00038	641.03
30	0.024	1.572	0.996	0.00048	648.57
40	0.03	1.877	0.978	0.0006	624.28
60	0.037	2.258	0.961	0.00074	606.79

Also, as the adsorbent bed particle size increased from 1.0 mm to 6.0 mm, the value of q_o decreased significantly, while the value of K_{Th} increases, the reason for the observed decrease in equilibrium amount of dye uptake per gram was that with increased in adsorbent bed particle size the accessible surface area to the adsorbate molecule reduces and thereby reducing its adsorption capacity (Moharir et al., 1980; Biswas and Mishra, 2015; Patel, 2019). Hence, lower flow rate, lower initial concentration, higher adsorbent mass and smaller adsorbent particle sizes would increase the adsorption of disperse azo dye on the granular composite activated carbon column. When flow rate increased from 85.0 mL/min to 115.6 mL/min, the 50% breakthrough time (τ) decreased and consequently, the amount adsorbed per gram of adsorbent decreases, while Yoon-Nelson rate constant K_{YN} increases, due to shorter residence time of the adsorbate molecule and increase in adsorbate saturation on the surface of adsorbent in the fixed bed column.

When the inlet concentration of dye increased from 50 mg/L to 200 mg/L, the 50% breakthrough time (τ) decreased from 34.1 to 9.1 mins and the amount adsorbed per gram of adsorbent (q_{OYN}) showed a sinusoidal trend, while Yoon-Nelson rate constant K_{YN} decreases (Table 4a). This is due to increase in driving forces for mass transfer, which lead to increase in saturation of the surface of adsorbent there by reducing adsorption rate and 50% breakthrough time (Patel, 2019). Also, with increase in adsorbent bed mass from 15 g to 60 g, the 50% breakthrough time (τ) increased and amount of adsorbate adsorbed per gram of adsorbent (q_{OYN}) also increased, while Yoon Nelson rate constant K_{YN} decreased, which may not be unconnected with the increase in available effective surface area of adsorbent, offering more site to adsorption, broadening the mass transfer zone. Furthermore, with increased in adsorbent particle size from 1.0 mm to 6.0 mm, the 50% breakthrough time (τ) and amount adsorbed per gram of adsorbent (q_{OYN}) decreased while Yoon Nelson rate constant K_{YN} increased. When adsorbent mass was fixed, increase in particle size invariably enhances fluid transportation down the column, thereby shortening the contact time and consequently, reduction in quantity of adsorbate adsorbed resulting (Patel, 2019).

4. CONCLUSION

In this study granular activated carbon was successfully prepared from rice husk and maize cob by carbonization and chemical activation using phosphoric acid. A mixture consisting of 70% MC and 30% RH showed higher surface area (796.8 m^2/g), 75.10% fixed carbon and moderate mesopores (32.69 Å) for adsorption. Maximum adsorption capacity of 84.11 mg/g was obtained in the bed using 50 mg/L inlet dye concentration, 20 g adsorbent mass, 85.0 mL/min adsorbate flow rate and 1.0 mm adsorbent particle size for the MC: RH 70:30 combinations. The dynamic adsorption behaviour of the bed showed that Thomas and Yoon-Nelson models are consistent with the data obtained in this investigation having R^2 values > 96% for most of the points, whereas the Adams-Bohart model showed corresponding values < 95%. The fixed-bed adsorption system was found to perform better with lower disperse azo inlet concentration, lower feed flow rate, higher activated carbon bed mass and smaller bed particle sizes.

5. ACKNOWLEDGMENT

The authors wish to acknowledge the assistance and contributions of the laboratory staff of Department of Chemical Engineering and Department of Chemistry, Ahmadu Bello University, Zaria, toward the success of this work.

6. CONFLICT OF INTEREST

There is no conflict of interest associated with this work.

REFERENCES

Ahmad, A.A and Hameed, B.H. (2010). Fixed-bed adsorption of reactive azo dye on to granular activated carbon prepared from waste. *Journal of Hazardous Materials,* 175(1-3), pp. 298-303

Ahmad, R. and Kumar R (2010). Adsorptive removal of Congo red dye from aqueous solution using bale shell carbon. *Applied Surface Science,* 257, pp. 1628-1633.

Bernal, V., Giraldo, L. and Moreno-Pirajan, J.C. (2018). Physicochemical properties of activated carbon: Their effect on the adsorption of pharmaceutical compounds and adsorbate-adsorbent interactions. *Journal of Carbon Research,* 62(4), pp. 1-8

Biswas, S. and Mishra U. (2015). Continuous fixed bed column study and adsorption modeling: Removal of lead ion from aqueous solution by charcoal originated from chemical carbonization of rubber wood sawdust. *Journal of Chemistry,* 2015, pp. 1- 9

Chen, J., Zhaang, L., Yang, G., Wang, Q., Li, R. and Lucia, L.A. (2017). Preparation and characterization of activated carbon from hydrochar by phosphoric acid activation and its adsorption performance in prehydrolysis liquor. *Bioresources,* 12(3), pp. 5928-5941

Cibele, C.O.A, Adriana, S.F. and Leandro, S.O. (2013). Removal of phenylalanine from aqueous solutions with modified corn cobs as adsorbents. *LWT – Food Science and Technology,* 51, pp. 1-8

Dusta, M., Buju, J.K., Faraz, M. D. H., Gautam, M. and Kumar, A. (2012). Fixed bed study of textile dye direct blue 86 by using a composite adsorbent 350-500 of azo dye on chitosan impregnated with a Cationic Surfactant. *International Journal of science and Engineering Research*, 6, pp. 536-545.

Ghribi, A. and Chlendi, M. (2011). Modeling of fixed bed adsorption: Application to the adsorption of an organic dye. *Asian Journal of Textile,* 1 (4), pp. 161-171

Goel, J., Kadirvelu, K., Rajagopal, C. and Garg, V.K. (2005). Removal of lead (II) by adsorption using treated granular activated carbon: Batch and column studies. *Journal of Hazardous Materials,* B125, pp. 211-220

Guo J. and Lua, A.C. (2003). Textural and chemical properties of adsorbent prepared from palm shell by phosphoric acid activation, *Materials Chemistry and Physics*, 80, p. 114–119.

Hadi, M., Samarghadi, M.R. and Mckay, G. (2011). Simplified fixed bed design models for the adsorption of acid dyes on novel pine cone derived activated carbon. *Water, Air and Soil Pollution*, 218(1), pp. 197-212.

Katheresan, V., Kansedo, J. and Sie-Yon, J.L. (2018). Efficiency of various recent wastewater dye removal methods: A review. *Journal of Environmental Chemical Engineering,* 6(4), pp. 1-8

Maneerung, T., Liew, J., Dai, Y., Kawi, S., Chong, C. and Wang, C.H (2016). Activated carbon derived from carbon residue from biomass gasification and its application for dye adsorption: Kinetics, isotherms and thermodynamics studies. *Bioresources Technology,* 200, pp. 350-359

Merzouk, B., Gourich B., Madani K., Vial, C. and Sekki, A. (2011). Removal of a disperse red dye from synthetic wastewater by chemical coagulation and continuous electrocoagulation. A comparative study. *Desalination*, 272, pp. 246–253.

Mitra, S., Muttakin, M., Thu, K. and Saha, B.B. (2018). Study on the influence of adsorbent particle size and heat exchange aspect ratio on dynamic adsorption characteristics. *Applied Thermal Engineering,* 133, pp. 764-773

Moharir, A.S., Kunzru, D, and Saraf, D. (1980). Effect of adsorbent particle size distribution on breakthrough curves for molecular sieve columns. *Chemical Engineering Science,* 35(8), pp. 1795-1801

Nsami, J.N and Mbadcam, J.K. (2013). The adsorption efficiency of chemically prepared activated carbon from cola nut shells by ZnCl2 on methylene blue. *Journal of Chemistry,* 2013, pp. 1-7

Patel, H. (2019). Fixed-bed column adsorption study: A comprehensive review. *Applied Water Science,* 9(45), pp. 1-17

Rahman, I.A., Saad, B., Shaidan, S. and Rizal E.S. (2005). Adsorption characteristics of malachite green on activated carbon derived from rice husks produce by Chemical-Thermal process. *Bioresources Technology*, 96(14), pp. 1578-1583

Rahman, M.M., Samsuddin, S.H., Miskon, M.F., Yunus, K. and Yusof, A.M. (2015). Phosphoric acid activated carbon as borderline and soft metal ions scavenger. Green Chemistry Letters and Reviews, 8(2), pp. 9-20

Ranga, S.V. and Sanghvi, L.K. (2015). Selection of adsorbent for removal of dye from wastewater. In: Proceedings of 2nd International Conference on Multidisciplinary Research and Practice, III(I), pp. 85-89

Rouf, S. and Nagapadma, M. (2015): Modeling of fixed bed column studies for adsorption of azo dye on chitosan impregnated with cationic surfactant. *International Journal of Scientific and Engineering Research*, 6(2), pp. 538-544

Shamsuddin, M.S, Yusoff, N. R.N. and Sulaiman, M.A. (2015). Synthesis and Characterization of activated carbon produced from kenaf core fiber using H_3PO_4 activation: A short review of bioreactor studies. *Water Resources*, 39, pp. 1425-1440.

Tan, L., Ning, S., Zhang, X. and Shi, S. (2013). Aerobic decolorization and degradation of azo dyes by growing cells of a newly isolated yeast *Candida tropicalis* TL-F1. *Bioresources Technology,* 138, pp. 307-313

Tay, T., Ucar, S. and Karagoz, S. (2009). Preparation and characterization of activated carbon from waste biomass. *Journal of Hazardous Materials*, 165, pp. 481-485.

Vadivelan, V. and Kumar, K.V. (2005). Equilibrium, kinetics, mechanism, and process design for the sorption of methylene blue onto rice husk. *Journal of Colloidal Interface Science*, 286, pp. 90-100.

Williams, P.T. and Reed, A.R. (2006). Development of activated carbon pore structure via physical and chemical activation of biomass fibre waste. *Biomass and Bioenergy,* 30(2), pp. 144-152

Yagub, M.T, Sen, T.K. and Ang, H.M. (2012). Equilibrium, kinetics, and thermodynamics of methylene blue adsorption by pine tree leaves. *Water, Air, and Soil Pollution,* 223, pp. 5267-5282.

Yagub, M.T., Sen, T.K., Afroze, S. and Ang H.M. (2014). Dye and its removal from aqueous solution by adsorption: A review. *Advanced Colloidal Interface Science*, 209, pp. 172-184.

Yunnen, C., Ye, W., Chen, L., Lin, G., Jinxia, N. and Rushan, R. (2017). Continuous fixed bed column study and adsorption modeling: Removal of arsenate and arsenite in aqueous solution by organic modified spent grains. *Polish Journal of Environmental Studies*, 26(4), pp. 1847 – 1854

Zhou, L., Li, M., Sun, Y. and Zhou, Y. (2001). Effect of moisture in microporous activated carbon on the adsorption of methane. *Carbon,* 39(5), pp. 773-776.